Award Number: W81XWH-10-2-0040

TITLE: Advanced Sensors for TBI

PRINCIPAL INVESTIGATOR: Bruce Lyeth, Ph.D.

CONTRACTING ORGANIZATION: University of California, Davis
Davis, CA 95616

REPORT DATE: December 2016

TYPE OF REPORT: Final

PREPARED FOR: U.S. Army Medical Research and Materiel Command
Fort Detrick, Maryland 21702-5012

REPORT DOCUMENTATION PAGE

Form Approved
OMB No. 0704-0188

1. REPORT DATE	2. REPORT TYPE	3. DATES COVERED
December 2016	Final	1 Jul 2010 - 30 Sep 2016

4. TITLE AND SUBTITLE
Advanced Sensors for TBI

5a. CONTRACT NUMBER
W81XWH-10-2-0040

5b. GRANT NUMBER

5c. PROGRAM ELEMENT NUMBER

6. AUTHOR(S)
Bruce Lyeth, PhD

E-Mail: bglyeth@ucdavis.edu

5d. PROJECT NUMBER

5e. TASK NUMBER

5f. WORK UNIT NUMBER

7. PERFORMING ORGANIZATION NAME(S) AND ADDRESS(ES)
University of California Davis
1820 Research Park Dr. STE300
Davis, CA 95616

8. PERFORMING ORGANIZATION REPORT NUMBER

9. SPONSORING / MONITORING AGENCY NAME(S) AND ADDRESS(ES)

U.S. Army Medical Research and Materiel Command
Fort Detrick, Maryland 21702-5012

10. SPONSOR/MONITOR'S ACRONYM(S)

11. SPONSOR/MONITOR'S REPORT NUMBER(S)

12. DISTRIBUTION / AVAILABILITY STATEMENT

Approved for Public Release; Distribution Unlimited

13. SUPPLEMENTARY NOTES

14. ABSTRACT
The major objective was to develop miniaturized, state-of-the-art pressure/temperature sensors to measure TBI impact intracranial pressure (ICP) combined with longer-term measurements of brain swelling biological ICP and intracranial temperature in animal models of TBI. The goal was to create new sensing technologies by modifying existing contract-stress pressure sensors developed at Lawrence Livermore National Laboratories (LLNL). Significant findings include the following. (1) The original LLNL sensors required a sealed reference volume over the sensor diaphragm to reliably detect pressures in a wet environment. (2) Original sensors were modified by epoxying an extremely thin layer of glass over the sensor diaphragm, creating a closed and sealed reference volume. This met with success in measuring TBI impact pressures and accurate temperatures, but lacked sensitivity for measuring the relatively small biological ICP. The increased size of sensor with the glass layer was not ideal. (3) Engineering calculations determined that a thinner diaphragm was necessary to reliably detect pressure changes in the brain swelling range of ICP. (4) The new wafer design and fabrication of the re-engineered sensors has been fraught with technical problems causing unfortunate delays.

15. SUBJECT TERMS
TBI, pressure, temperature, sensors, ICP

16. SECURITY CLASSIFICATION OF:			17. LIMITATION OF ABSTRACT	18. NUMBER OF PAGES	19a. NAME OF RESPONSIBLE PERSON
a. REPORT	b. ABSTRACT	c. THIS PAGE			USAMRMC
Unclassified	Unclassified	Unclassified	Unclassified	29	19b. TELEPHONE NUMBER *(include area code)*

TABLE OF CONTENTS:

INTRODUCTION:

The fundamental problem studied is this seed project was to examine what pressure changes are transmitted into and through the brain by traumatic brain injury (TBI). Virtually nothing is known about rapid pressure changes in the brain during impact TBI. This project proposed to use state-of-the-art pressure sensors engineered at Lawrence Livermore National Laboratory (LLNL) to measure rapid pressure changes in the fluid percussion model of TBI in rats. The LLNL sensors were designed to be extremely small with micro-second time resolution.

The major objective of this project is to create new sensor technologies and perform preliminary studies in an impact model of TBI for subsequent rapid transition to testing in blast TBI models with future funding opportunities. The hypothesis was that measurement of intracranial pressure transients in an impact model of traumatic brain injury will provide valuable data about sensor performance within a biological system that will be directly applicable to subsequent transition into blast TBI animal models.

The Specific Aims of this project were: 1) to evaluate existing prototype micro pressure sensors from LLNL in the rat fluid percussion impact TBI model, and 2) to design and evaluate second generation LLNL multimodal micro pressure sensors (impact wave, biological ICP, and temperature) in the fluid percussion rat impact TBI model.

The study design of this seed project proposed to use miniaturized, state-of-the-art pressure/temperature sensors engineered at the LLNL to measure the immediate increases in intracranial pressure (ICP) combined with longer-term measurements of biological ICP (associated with brain swelling) and intracranial temperature. Experiments were to utilize the placement of sensors at strategic locations within the calvarium in order to obtain the most rigorous measure of acute transmission of pressure waves through the brain, and reflection/rebound pressure waves within the cranium as well as longer-term changes in biological ICP, and intracranial temperature.

The significance of this project lies in the development of an advanced multi-modal sensor design that can be used to measure the transfer of kinetic energy from a pressure wave from impact or explosion to brain tissue in a living animal. The proposed studies represented a critical initial step in this process. The proposed experiments were designed to test novel sensors developed at LLNL in a rat impact TBI model (fluid percussion) in order to evaluate and troubleshoot a number of issues associated indwelling sensors in the brain. The use of the rodent impact TBI for initial characterization and troubleshooting of the multimodal sensors represented an efficient time- and cost-effective strategy to allow for a smooth transition into larger animals. Better understanding the mechanics and the pathophysiological and functional consequences of TBI should promote innovation that will lead to widespread use of this device by the Neurotrauma community for modeling and studying battlefield TBI and ultimately to the design of enhanced protection as well as improved pharmacological treatment for blast-injury victims and civilians as well.

KEYWORDS:

Pressure Sensors, Traumatic Brain Injury, ICP, Fluid Percussion, Temperature

ACCOMPLISHMENTS:

We performed initial static calibration curves for the existing LLNL sensors in both dry and wet environments.

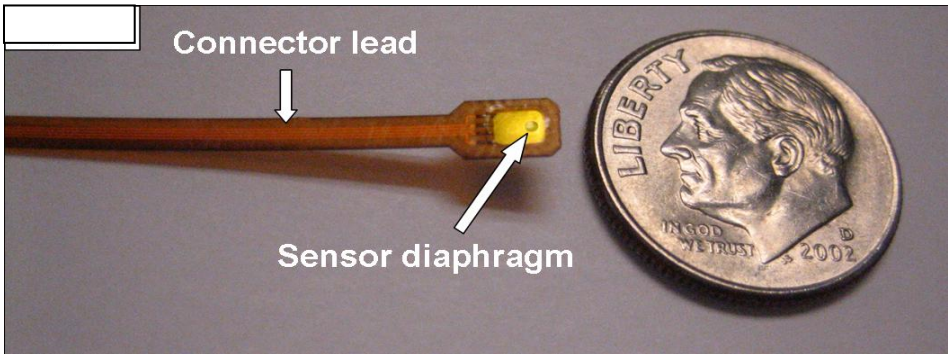

Figure 1: Photograph of original LLNL microsensor. The sensor diaphragm was packaged with a connector lead and exterior protective coating.

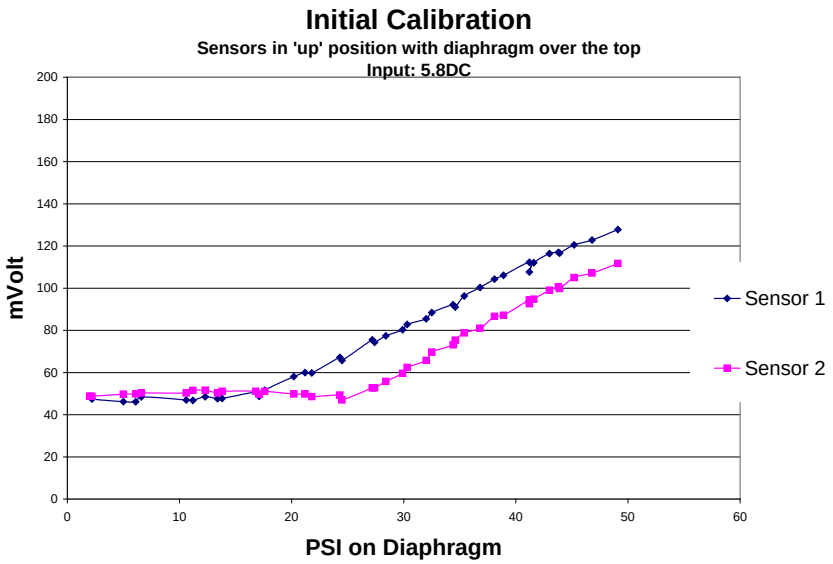

Figure 2. Dry static pressure calibration: Changes in sensor output voltage were recorded over a range of pressures applied to the sensors. Note that the sensors were unresponsive to pressures under 20 PSI. Between 20 and 50 PSI both sensors produced a linear response to increasing pressure.

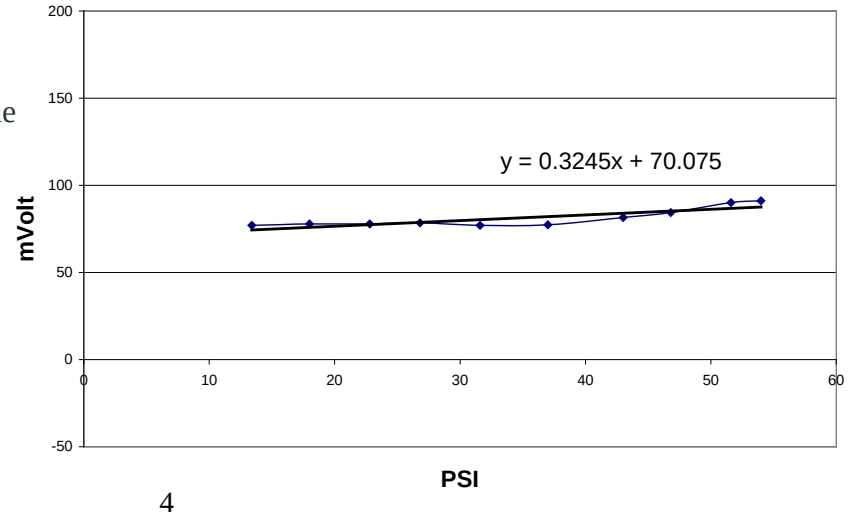

Figure 3. Wet condition static pressure calibration: Changes in sensor output voltage were recorded over a range of pressures applied to the sensors. Note that this sensor was unresponsive to changes in applied pressures. Furthermore, we found that these sensors were irrevocably damaged from fluid leakage. Sensor redesign was necessary to solve this problem.

We encountered significant problems associated with the lack of response of the exiting LLNL sensors in a wet environment. We found that the existing LLNL pressure sensors were limited in their ability to detect pressure transients in a wet environment. We determined that a sealed reference volume over the sensor diaphragm would be required in order to reliably detect pressures in a wet environment across a range of impact and blast TBI pressures. After considerable experimentation with a variety of backing materials and epoxy methodologies, we were able to successfully overcome this limitation.

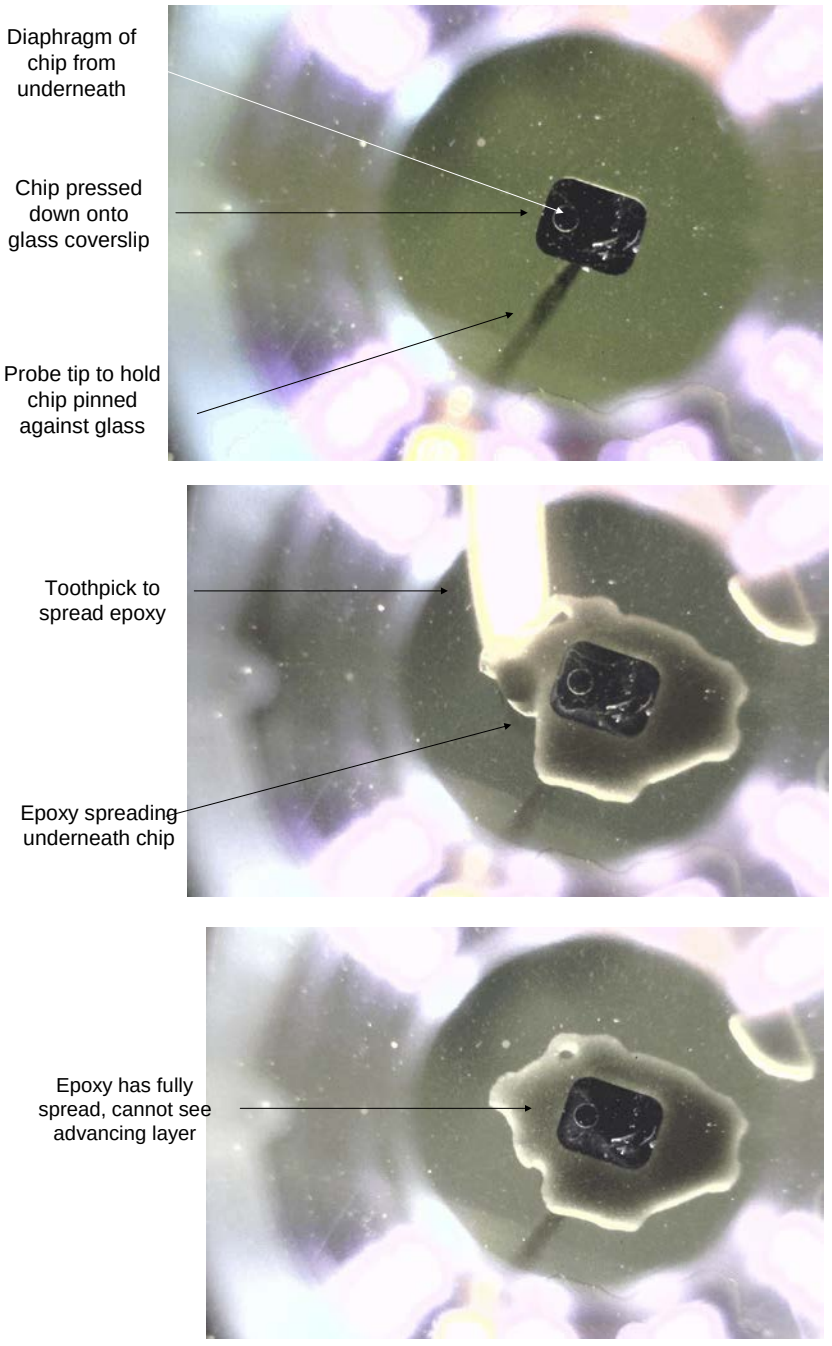

Figure 4. Creating a sealed reference volume: We successfully enclosed a reference volume on the pressure sensor, enabling the contact pressure sensors to be placed in a fluidic environment and detect a change in pressure. The epoxy application process procedure is shown for enclosing an extremely thin layer of glass over the sensor diaphragm, creating a closed and sealed reference volume. All three views are taken from beneath the setup looking upward, through the transparent glass coverslip onto the backside of the chip. The top picture shows the setup of the procedure before epoxy was applied. The middle picture shows the epoxy spreading across the backside of the chip, as an advancing front of epoxy can be seen. The lower picture shows the chip after the epoxy has finished spreading, contacting the entire backside of the chip but not the diaphragm. During the curing process the liquid epoxy is heated to ensuring a strong bond and a hermetic seal. The excess glass coverslip is later precisely trimmed away with a special dicing saw.

LLNL designed and built a test chamber to evaluate and characterize the unpackaged sensors. A pressure chamber was designed and fabricated to both create an electrical connection to the chip and allow connection to the fluid percussion instrument, enabling us to measure the dynamic characteristics of the sensor.

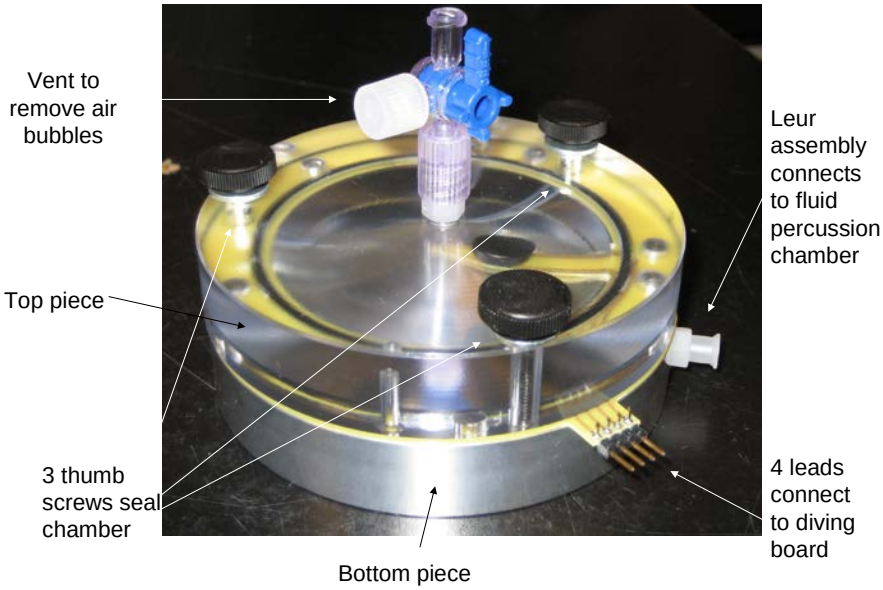

Figure 5. Fluidic test chamber: LLNL machined a fluidic test chamber for bench-testing and characterizing pressure responses of sensors. The chamber consisted of a two-piece assembly with an aluminum base and clear Plexiglas dome that allowed visualization of sensor and detection of air bubbles within the test chamber.

We performed impact pressure recording from sensors within the fluidic test chamber.

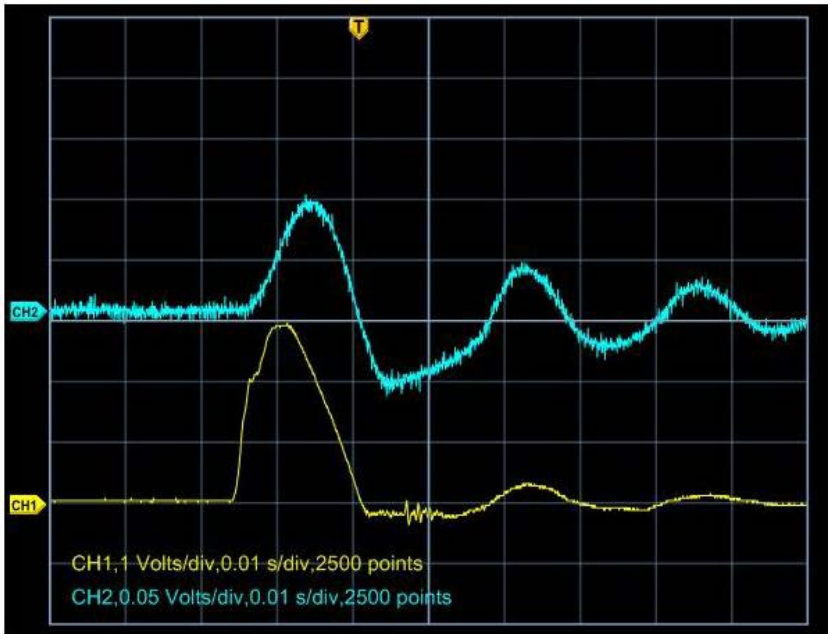

Figure 6. Dynamic pressure recordings: This figure shows the dynamic pressure tracing of a sensor with an enclosed reference volume. The test chamber (Figure 5) with sensor chip was connected to the fluid percussion device through the Luer fitting. The chamber was subjected to a fluid percussion impact. The screenshot shows the LLNL sensor signal in the blue upper trace and the standard fluid percussion pressure transducer signal in the yellow, lower trace. Each division on the X-axis is 5 msec. Note the high correspondence of the LLNL sensor to the FP transducer. Also note the amplified secondary

waveforms. We discovered a trapped bubble in the test chamber that caused the rebounding secondary pressure changes. Not only did the sensor respond, but it was undamaged from repeated tests indicating a functional seal of the enclosed reference volume.

We performed evaluation of brain responses (e.g. cell death, glial scarring) to sensors implanted for 14 days in four different intracranial locations.

Figure 7. Gross morphology from implanting sensors: We implanted sensors in different locations within the rat skull/brain to determine brain tissue reactions to the implants. The sensors remained implanted for 14 days. The gross pathology of the brain shows that implant configurations 1 and 2 (subdural placement) resulted in the greatest gross infarction on the surface of the cortex while implant configurations 3 and 4 (epidural) showed essentially no gross pathology.

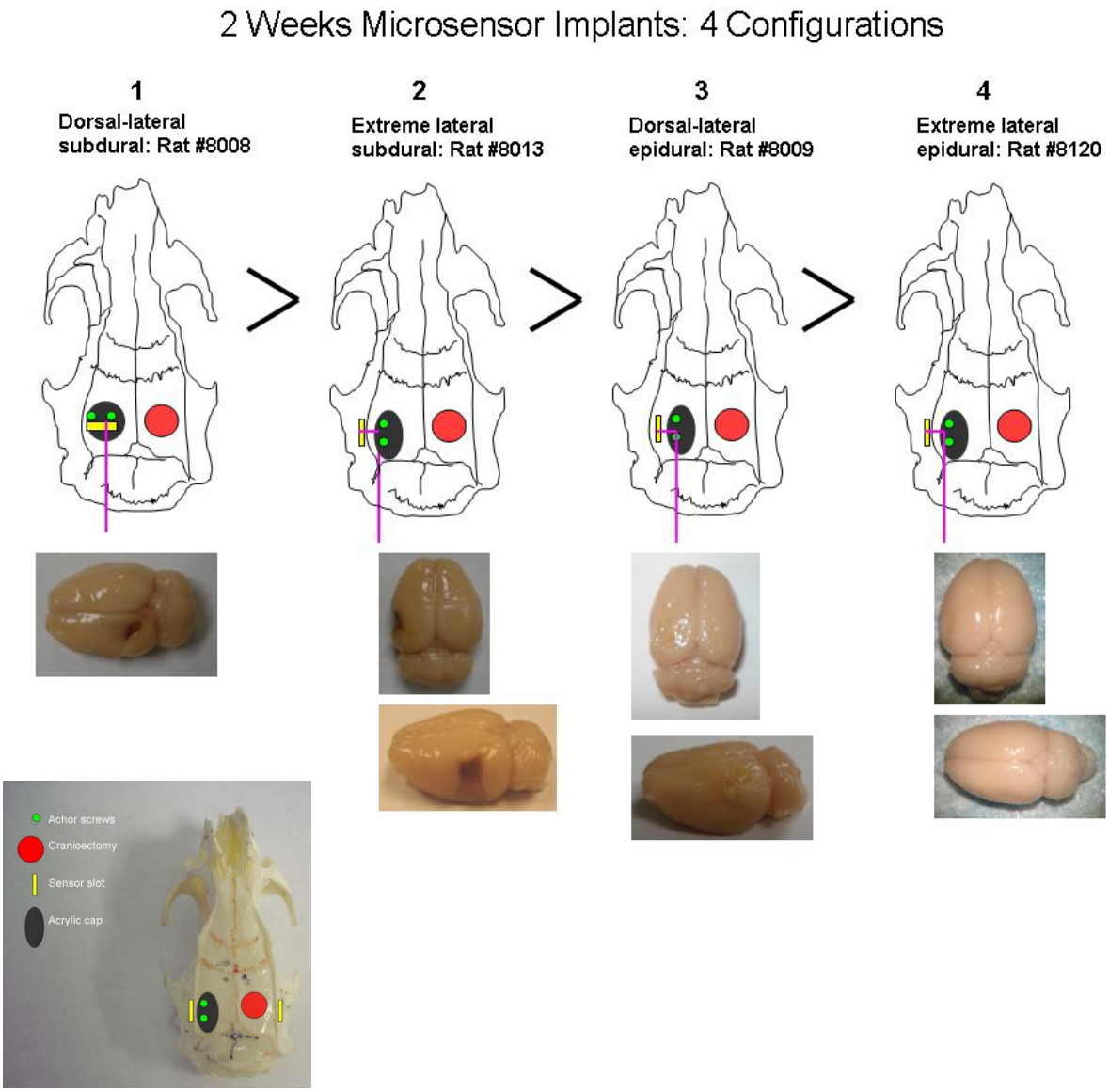

Figure 8. Cresyl-violet histology: Histology was performed to examine areas of brain tissue infarct in response to sensor placement in each of the four implant configurations. The sensors remained implanted for 14 days. The tissue was then sectioned and stained with Cresyl-violet. In configurations 1 and 2, histological stains showed infarction (2X objective, black arrows) localized to the implant site. For configuration 3, there was less tissue damage and with configuration 4 there was minimal evidence of cortical damage with cresyl violet staining.

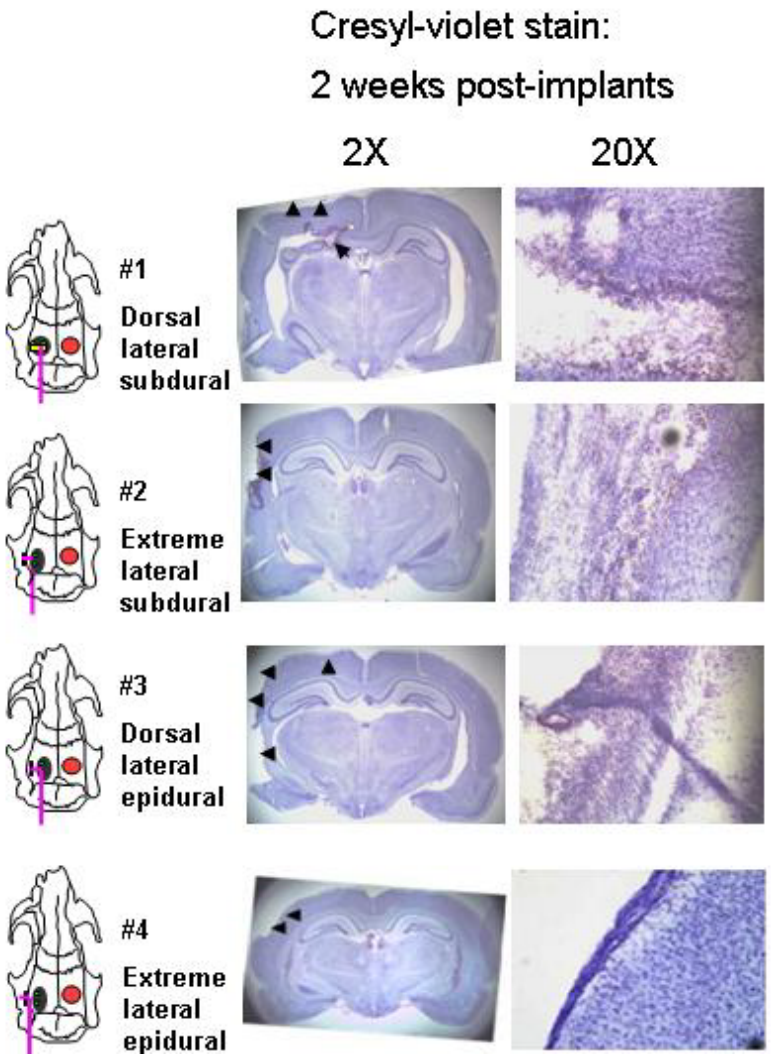

Figure 9. Microglia histology: Further histology was performed to examine microglia reaction using a microglia –specific antibody (anti Iba-1) as an indicator of inflammatory responses to sensor placement in each of the implant sites. Configurations 1 and 2 showed the greatest inflammatory response (20X objective) localized to the implant site.. Configuration 3 had minimal infiltration of activated microglia.

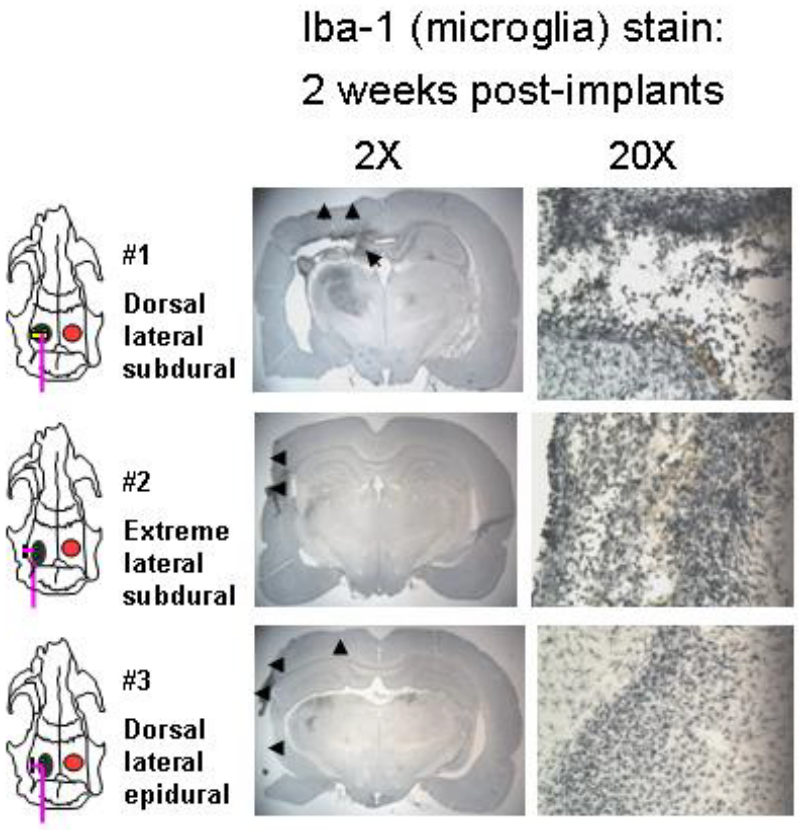

Figure 10. Body weight measurements: Body weight was used as an indicator of general health of the rat. The different sensor implantation configurations produced very different body weight responses over the 2-week period. The extreme lateral epidural implanted animals (Configuration 4) showed the greatest recovery in body weight (green line).

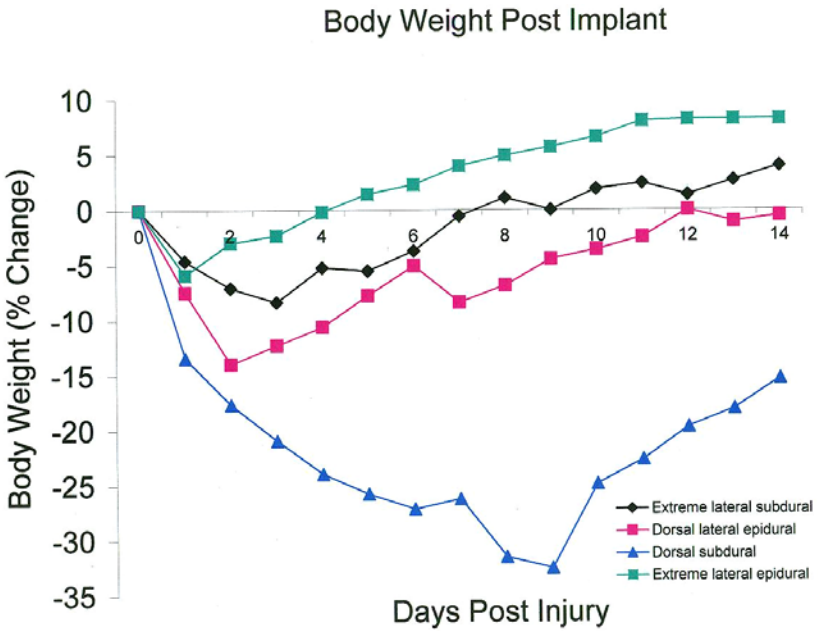

We implanted the packaged sensors which were modified with the glass-enclosed sealed reference volume into the brain of rats and subjected them to varying magnitudes of fluid percussion TBI.

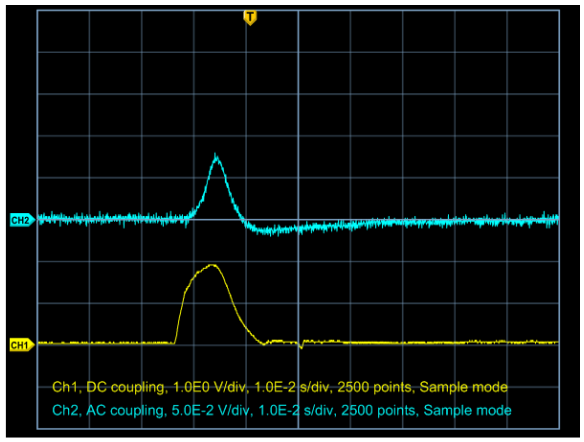

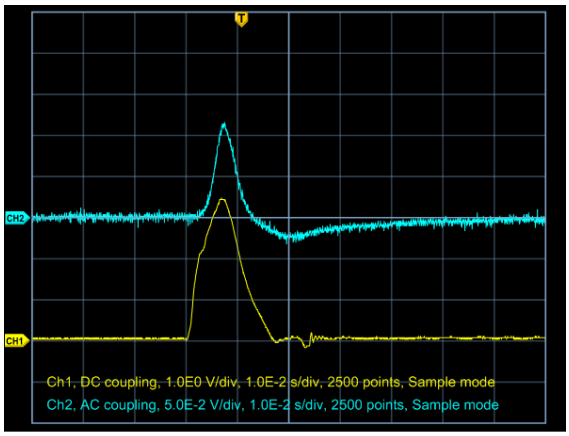

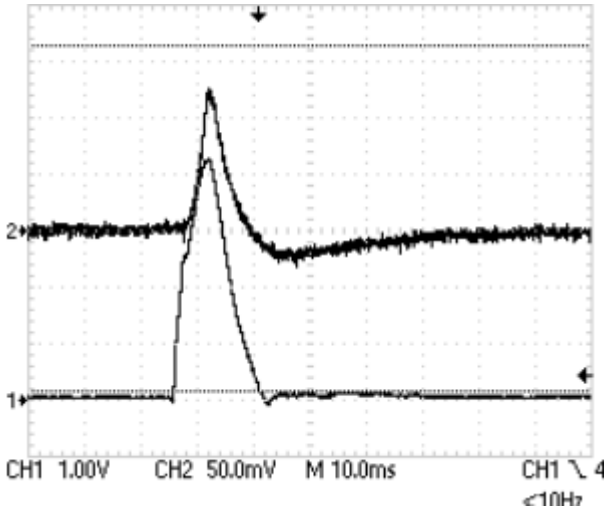

Figure 11. In vivo pressure measurements: The three oscilloscope screenshots show the LLNL sensor's signals plotted simultaneously with the fluid percussion reference pressure transducer signal following mild (upper screenshot), moderate (center screenshot), or severe (lower screenshot) fluid percussion TBI in the rat. The LLNL sensor was placed within the rat's skull in a lateral epidural position. While it appears that the fluid percussion reference sensor has a greater sensitivity to pressure than the LLNL sensor, this difference is actually due to the different voltage output characteristics of the fluid percussion pressure transducer and the LLNL sensor. There is also some force reduction as the dynamic pressure wave travels through the Luer fitting into the rat's cranial vault. Overall, these data demonstrate that dynamic measurements with the LLNL sensor can be performed with a high level of precision and that the modified LLNL sensor readings correspond to the upstream fluid percussion reference pressure transducer. It is also noteworthy that the LLNL sensor's peak signal occurs slightly after that of the fluid percussion reference transducer peak signal. This is due to the LLNL sensor being located "downstream" of the reference sensor, as the dynamic pressure wave will reach the reference sensor before it reaches the LLNL sensor.

We attempted to perform extended biological ICP recording from sensors implanted in the brain of rats subjected to varying magnitudes of fluid percussion TBI. However, we

encountered a limitation of the existing LLNL sensors in that they were not sensitive enough to detect the relatively small pressure changes (10-40 mm Hg or less than 1 psi) associated with biological ICP from brain swelling. Even with the incorporation of the reference volume over the sensing diaphragm, static pressure testing was not able to reliably detect pressure changes within the brain swelling range. As detailed in Figures 12 & 13, our collaborating engineers determined that a thinner diaphragm could solve this problem.

Figure 12. Engineering calculations to increase sensitivity: Engineering calculations were performed to predict how a change in thickness of the LLNL sensor diaphragm could increase the sensitivity to low pressures encountered with changes in biological ICP (less than 1 psi). α1 and α2 correspond to the change in resistance divided by the nominal resistance of the resistor. πl and πt correspond to the longitudinal and transverse piezoresistive coefficients of boron doped silicon. ν is the poisson's ratio. Thus, the larger the radius and the thinner the diaphragm, the larger the radial stress and the larger the voltage output to an applied pressure. This is plotted in the graph below (Figure 13).

$$Vout = Vin\frac{2*(\alpha_1+\alpha_2)}{1+\alpha_1-\alpha_2}$$

$$R1 = R4 = R0*(1+\ \alpha_1)$$

$$R2 = R3 = R0*(1-\alpha_2)$$

$$\alpha_1 = \ \sigma_r*(\pi_l+\nu*\pi_t)$$

$$\alpha_2 = -\sigma_r*(\pi_t+\nu*\pi_l)$$

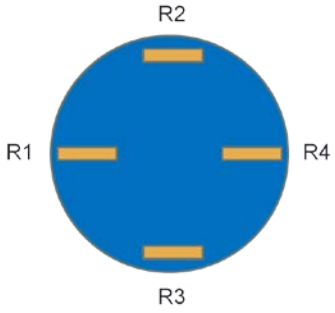

Equations from MAE 229 MEMS Design

UCDAVIS COLLEGE OF ENGINEER

Calculation of σr

- From Timoshenko, Theory of Plates and Shells:
- This is valid only at the outer edge of the plate, and for small deformations
- σr = radial stress
- P = uniformly applied pressure
- r = radius of the plate
- t = thickness of the plate

UCDAVIS COLLEGE OF ENGINEERING

Figure 13. Voltage output vs. diaphragm thickness: The plotted points were derived from the following parameters: a 500 micrometer diameter diaphragm, 1 mmHg applied, 5V as the input, and πl = 71.8e-11, πt = -66.3e-11. Thus, it appears that we would want to select a diaphragm with a thickness of 1 micrometer and a diameter of 500 micrometers.

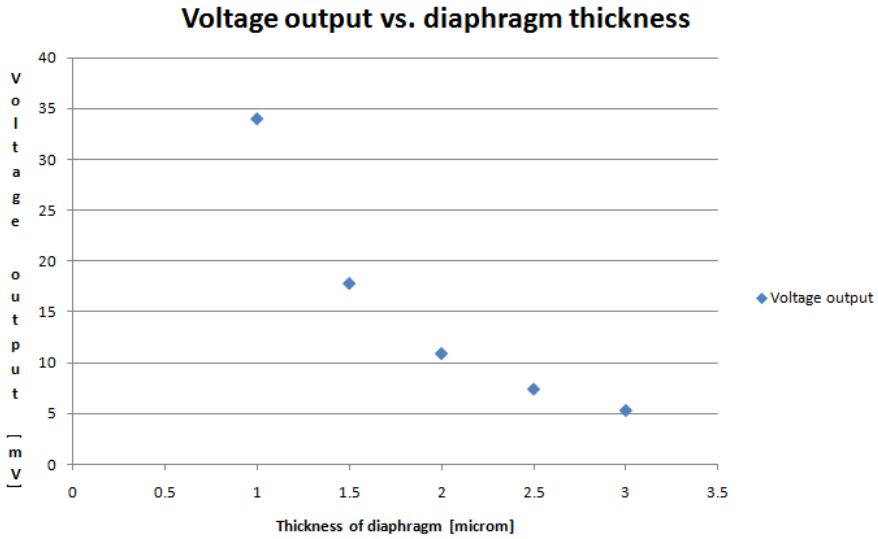

However, one of the consequences of thinning the diaphragm is that it is more likely to burst when exposed to the large 50 psi pulse it will experience during an actual TBI or blast.

Figure 14. Simulations: The Von Mises Stress for an applied load of 50 psi was determined using COMSOL Multiphysics, a finite element modeling program. The picture shows a simulation of the diaphragm bending for a 3 micrometer thick diaphragm. The rainbow gradient shows the deflection of the diaphragm, with red being the largest deflection and blue being the smallest.

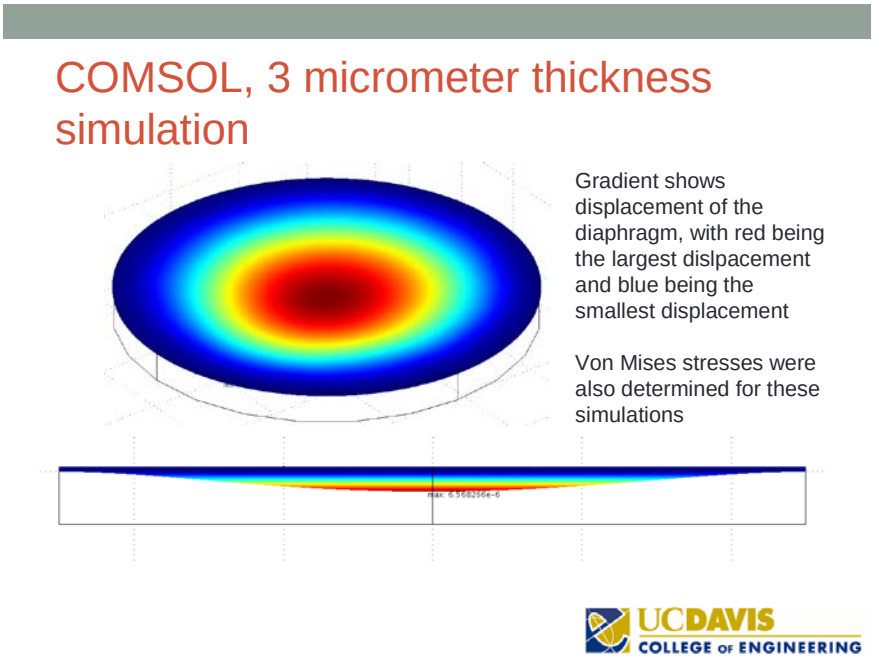

The Von Mises Stresses were determined for a number of diaphragm thicknesses, and are plotted below:

Figure 15. Summary of simulations: The black horizontal line plotted in the graph shows the yield stress of silicon single crystal. Because the Von Mises Stress of the 1 and 1.5 micrometer thick diaphragms exceeds the yield stress, these diaphragms would permanently deform and possibly burst when exposed to a blast of 50 psi. Thus, dimensions of 500 micrometer diameter and 2 micrometer thickness seem to be optimum in surviving the 50 psi

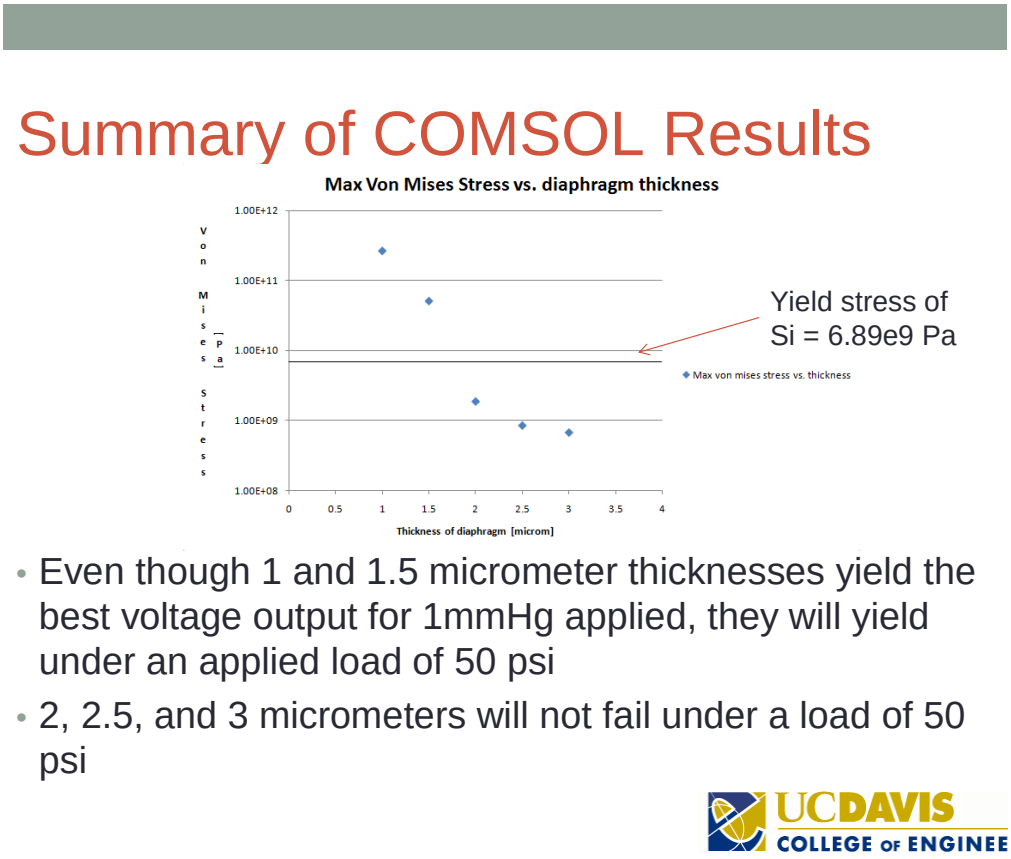

blast without incurring damage and still being capable of measuring a pressure of 1 mmHg with acceptable accuracy. These dimensions yield a signal to noise ratio of 7 for a 1 mmHg load, and a safety factor of 3.7 during the 50 psi blast. However, in order to create a sensor with these dimensions, we would need to perform a re-fabrication of the sensor.

We performed engineering calculations for measurement of temperature with the LLNL pressure sensor. Design and experiment modifications were performed that lead to the ability to measure temperature. It is often desirable when making pressure measurements to be able to isolate the voltage increase due to pressure change from the voltage increase due to temperature change. This is accomplished using temperature compensation, as shown in the Figure 16 below:

Figure 16. Temperature Compensation: All resistors experience the same change in resistance when heat is applied making the Wheatstone bridge temperature compensating. This is advantageous as it allows one to measure a pressure independent of the temperature of the device.

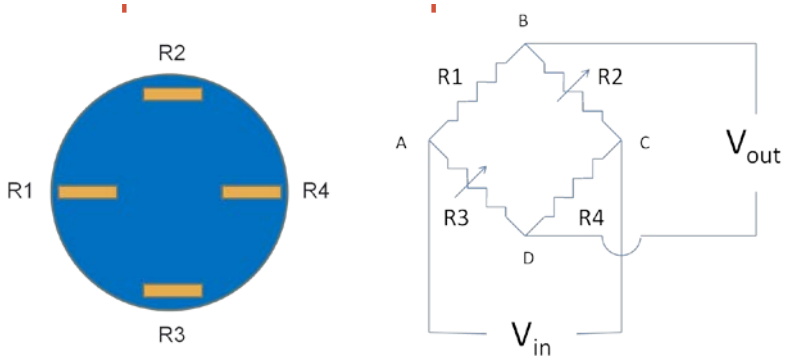

• All resistors experience the same change in resistance when a temperature is applied, so the bridge is temperature compensating
• This is advantageous, as it allows us to measure a pressure independent of the temperature the device is exposed to

$$Vout = Vin\left\{\frac{R1R4 - R2R3}{(R1 + R2)(R3 + R4)}\right\}$$

UCDAVIS COLLEGE OF ENGINEERING

Figure 17. Temperature Sensing: The voltage output from the Wheatstone bridge is due to a pressure increase only, as temperature change will cancel each other out, as the numerator should remain zero unless a pressure is applied. This is advantageous for pressure measurements but not for temperature measurements. Temperature measurements can be made by shorting across R1 and R4, and measuring the resistance change of R2 and R3, which are now in parallel.

- This is advantageous for measuring pressure independent of temperature, but is not useful for measuring temperature
- To measure temperature, we must modify the setup to no longer be temperature compensating
- This is accomplished by shorting across R1 and R4

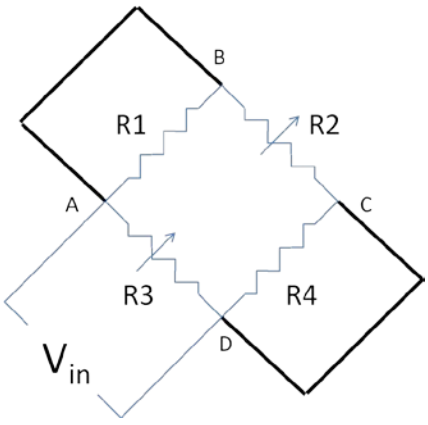

Figure 18. Temperature Sensing Circuit: The bridge and subsequent resistance change are presented in the formulas.

- The wheatstone bridge can be redrawn as shown below
- We can apply an input voltage and measure the current change across the resistors

$$Req = \frac{R2R3}{R2 + R3}$$

$$R = \frac{(R2 + \Delta R)(R3 + \Delta R)}{R2 + R3 + 2\Delta R}$$

$$R = \frac{R2R3 + \Delta R(R2 + R3) + \Delta R^2}{R2 + R3 + 2\Delta R}$$

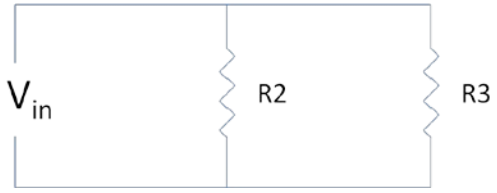

UCDAVIS COLLEGE OF ENGINEERING

Figure 19. Temperature Measurements: We incorporated these changes and have successfully measured temperature with the rewiring of the circuitry described above. A temperature calibration curve was derived for the modified LLNL sensor. Note the linear correspondence between temperature and output amperage. There was a high degree of correlation (R>0.99) which should produce a highly reliable measurement of brain temperature using the modified circuitry.

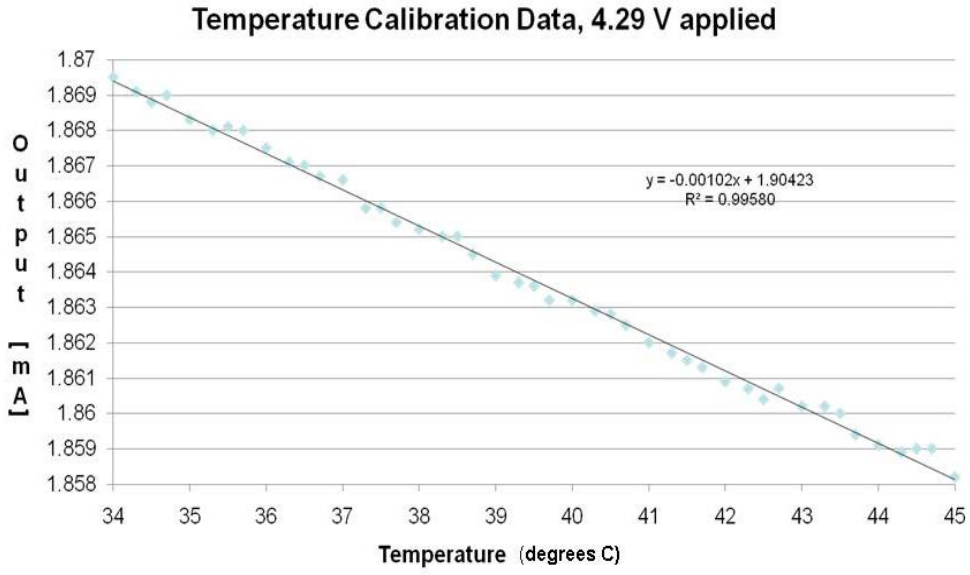

Dr. Kotovsky successfully produced test-ready sensors with a range of diaphragm diameters (200, 400, 600, 800, and 1000 μm diameter). Diaphragm diameter should affect sensitivity of the sensors. These wafer-scale, absolute pressure sensors had an ultra-thin form factor (thickness 90 μm prior to packaging and 130 μm after final packaging). The new sensors were designed to measure absolute pressure by modifying the original contact stress sensor design to create a reference cavity; a trapped volume of gas that is hermetically sealed within the device. The new sensors pre-define the pressure sensor's reference cavity within the Silicon-on-Insulator (SOI) wafer. The pre-definition provides a variety of advantages to the overall process:

Bench calibration and testing of sensitivity were completed. Five new sensors with diaphram diameters of 200, 400, 600, 800, and 1000 μm (Figures 20 & 21) were tested and calibrated to determine the optimum diaphragm diameter for subsequent in-animal testing. The new sensors were packaged with an encapsulating layer of Kapton to protect the sensor diaphragm and electrical connections from body fluids.

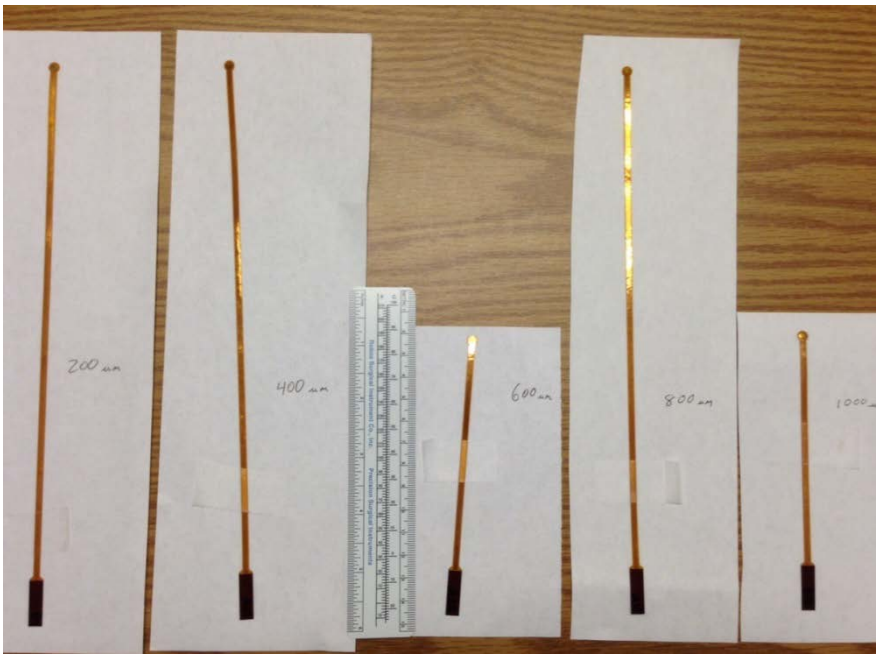

Figure 20. Sensors with different diaphragm diameters. The overall length of the sensor and connecting contact strip are either 13 or 25 mm.

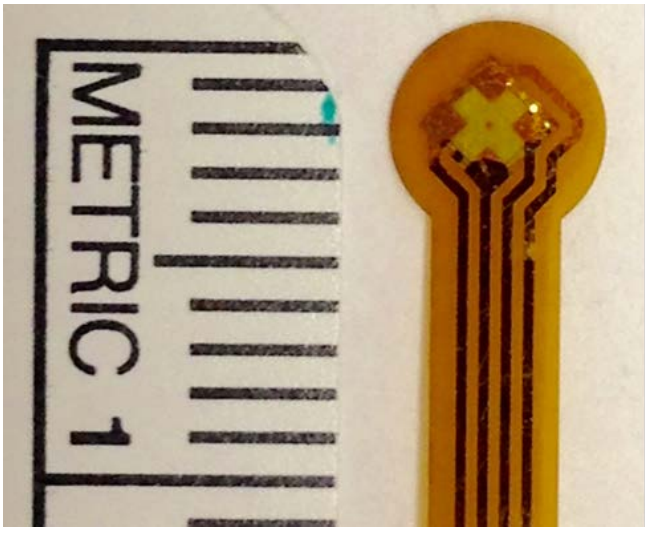

Figure 21. Sensor: Close-up photo of sensor showing diaphram and 4-lead connector contact strips.

We used a redesigned test chamber (Figure 22) machined by Dr Kotovsky that provided a means of ex-vivo static and dynamic pressure testing of packaged sensors. The chamber is a two part assempbly with an aluminum base and clear Plexiglas top with a 2 mm^3 internal volume that simulates the voume of an adult rats brain. One inlet and one outlet port allow for filling with distilled water and efficient removal of air bubbles. The inlet port is a female Luer fitting that also allows for application of static pressure for calibration as well as connection to the fluid percussion device for dynamic testing.

Figure 22. Test chamber for ex-vivo testing and calibration of sensors.

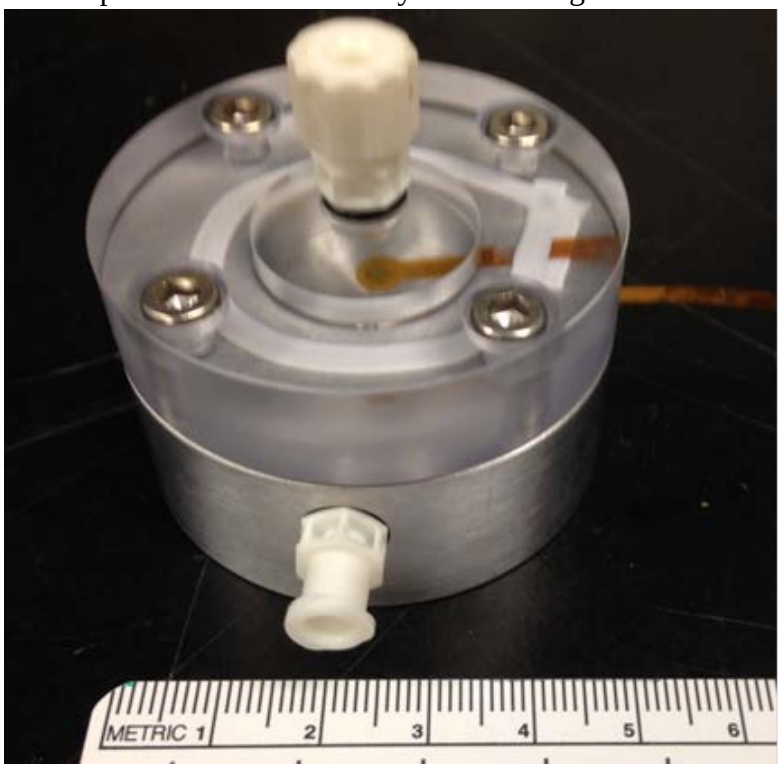

We performed static pressure calibration on the 200, 400, 600, 800, and 1000 μm diameter diaphram sensors (Figures 23 - 27). The 200 and 400 μm diameter diaphram sensors had a linear pressure-voltage rsponse only between 15 and 30 psi. At lower or higher pressures, the sensors respoinded poorly. Thus, their lack of sensitivity precludes use of these diamter diaphram sensors for further testing. In contrast, the larger diameter diaphram sensors were linesar throughout the 0-50 psi calibration range. We proceeded to use of the 1000 μm diameter diaphram sensors in subsequent experiments.

Figure 23. Static calibration of 200 μm diameter diaphram sensor.

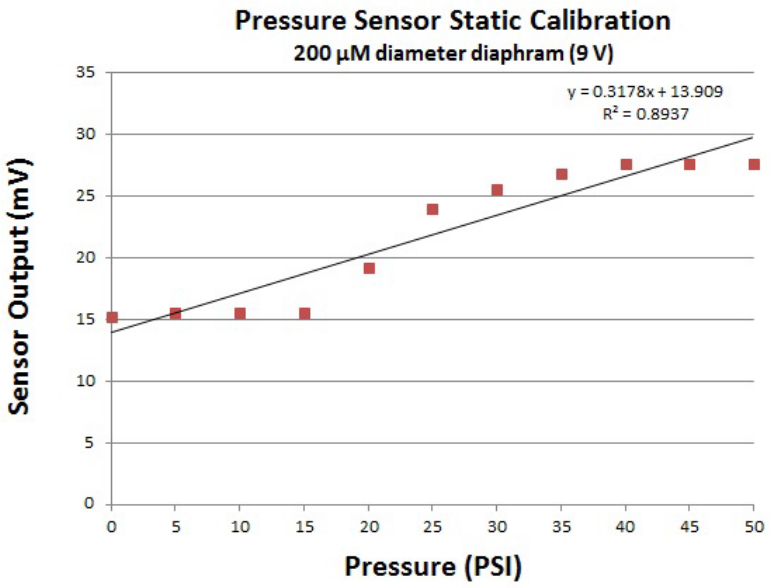

Figure 24. Static calibration of 400 μm diameter diaphram sensor.

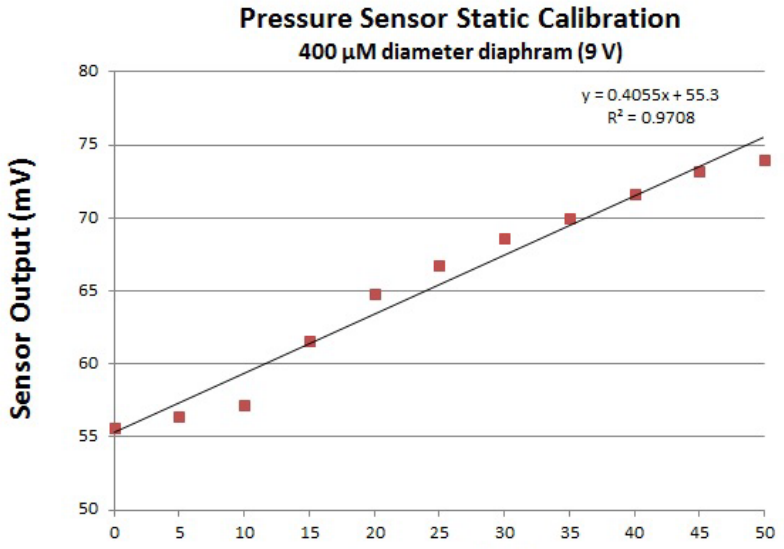

Figure 25. Static calibration of 600 μm diameter diaphram sensor.

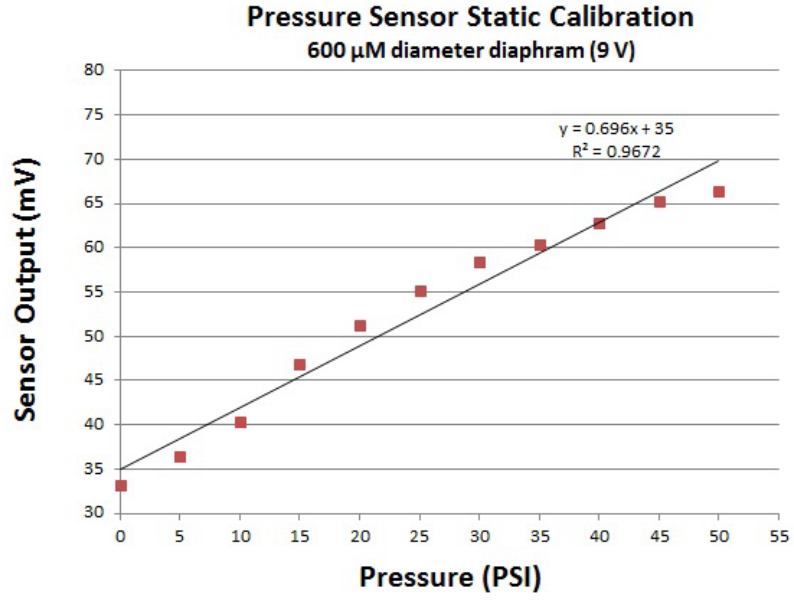

Figure 26. Static calibration of 800 μm diameter diaphram sensor.

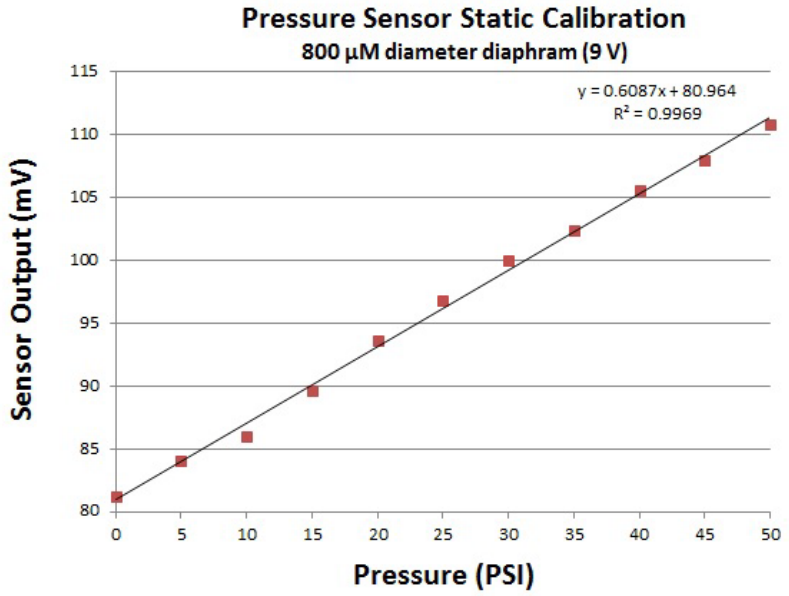

Figure 27. Static calibration of 1000 μm diameter diaphram sensor.

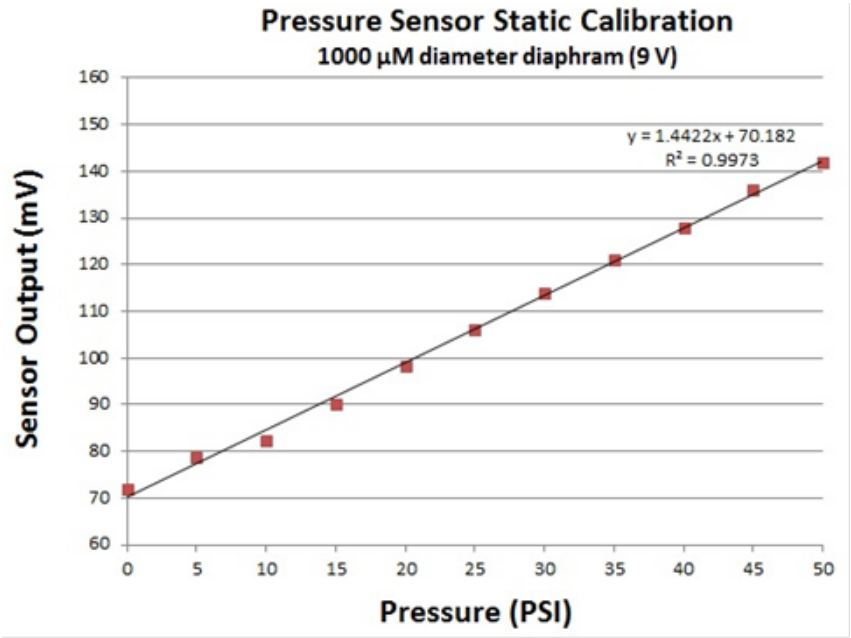

We performed an initial dynamic pressure comparison of the new 1000 μm sensor to the existing pressure transducer on the fluid percussion device (Figure 28) using the new test chamber connected to the fluid percussion device. The new sensor tracked changes in pressure over time that were in close agreement with the exisitng pressure transduceer on the fluid percussion device. Electrical shielding of the cables improved the signal-to-noise response compared to previous dynamic testing.

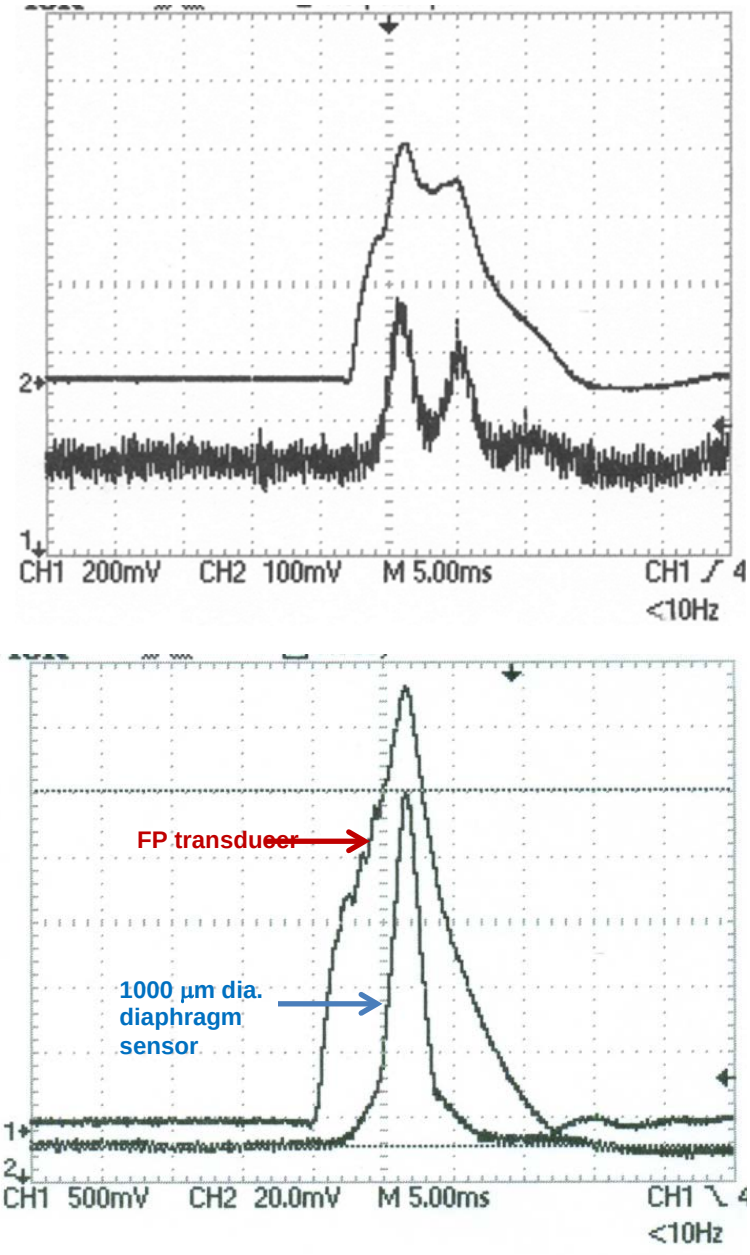

Figure 28. Ex vivo Dynamic Testing: Comparison of fluid percussion pressure transducer (upper trace) and new 1000 μm diameter diaphram sensor (lower trace). Note the lower panel showing the improved signal-to-noise response after the electrical cables were shielded.

We next implanted a 1000 mm diamter diaphram sensor into the cortex of a rat (Figure 29) and subjected the animal to a moderate fluid percussion TBI. We simultaneously recorded dual traces from the brain-implanted sensor and the standard pressure transducer located near the outlet of the fluid percussion device. The implanted sensor recorded a higher pressure than the external pressure traansducer on the fluid percussion device (Figure 30).

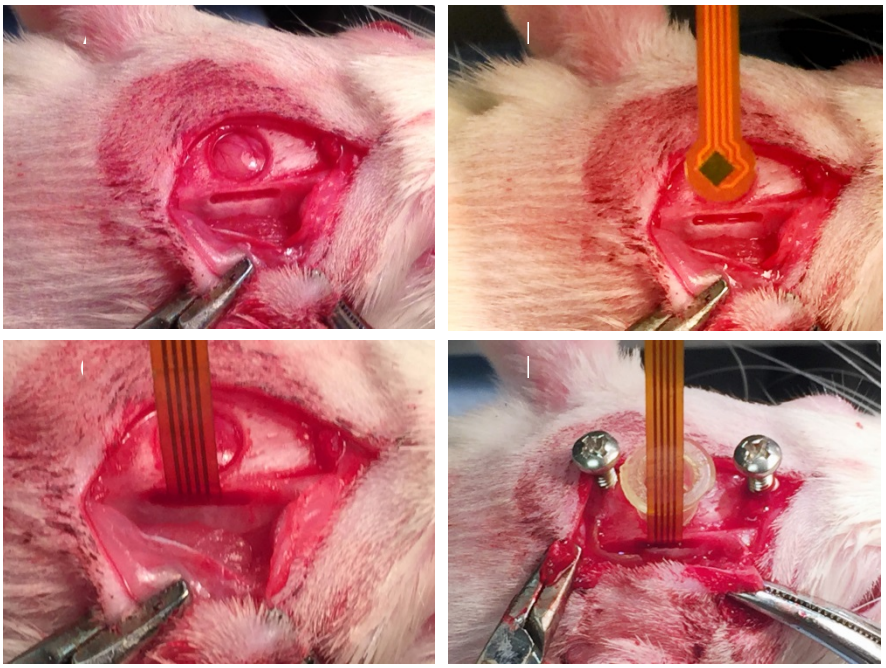

Figure 29. Implanting sensor: Implanting the sensor into the cortex of a rat prepared for fluid perussion TBI. An incision was made in the scalp on the dorsal surface of the rat's head. A circular craniotomy was performed for induction of the fluid percussion and a slot was drilled in the skull for insetion of the sensor into the cortex. The sensor was lowered into the slot and enterd the cortex. The surgery was completed by attaching the fluid percussion cannula to the craniotomy and anchored in place with two skull screws. Dental acrylic was then applied to hold the entire assembly in place.

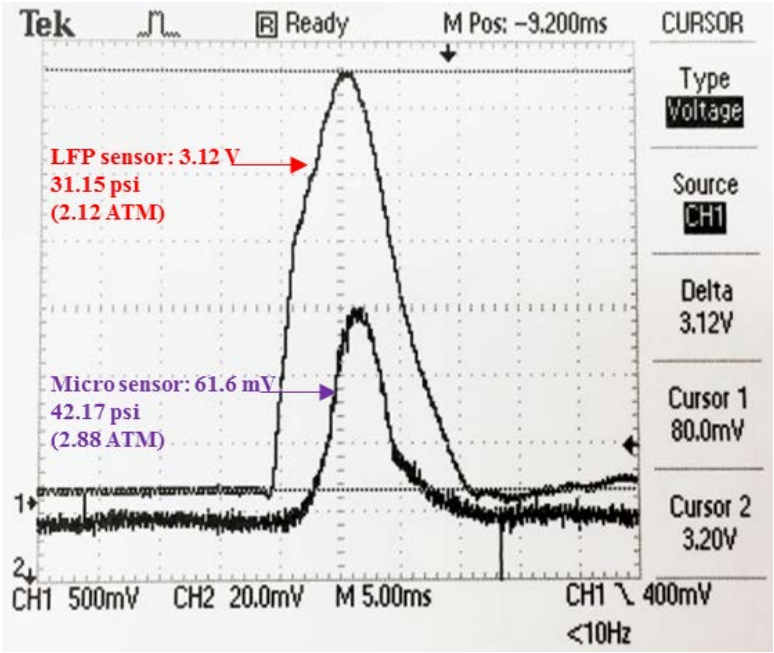

Figure 30. In vivo dynamic testing: Comparison of fluid percussion device pressure transducer (upper trace) located near the outlet of the device and new 1000 μm diameter diaphram sensor (lower trace) implanted into the cortex of the animal.

Conclusions from closed diaphragm sensors

- The first production of closed diaphragm wafer sensors were received from Lawrence Livermore National Laboratories and extensively tested.
- Static calibration produced a linear relationship between 0 and 50 PSI for the larger diameter diaphragm sensors (800 & 1000 μm diameter) with an $R^2 = 0.986$
- The closed-diaphragm sensor is 90 microns thick and the final product with Kapton packaging is 130 microns thick
- Dynamic comparison of the new sensor with the existing fluid percussion pressure transducer provided close tracking of pressure events.
- Initial testing revealed that electrical shielding of cables and power supply provided reduced noise and thus a greater signal-to-noise ratio.
- Initial testing with sensor implanted in rat cortex was successful.

Limitations of the closed diaphragm sensors

A major shortcoming of the modified original sensors was the inability to measure very low pressures associated with biological ICP from brain edema (10-40 mmHg; less than 1 psi). Engineering calculations indicate that a thinner sensor diaphragm wouldl make such small pressure measurements feasible without compromising high pressure measurements associated with blast TBI. The third generation sensor was planned to be designed and fabricated for the option year of this project. Dr. Kotovsky at LLNL worked diligently on re-engineering the previous sensor by designing a new generation sensor capable of reliably detecting very low pressures (10-40 mmHg or < 1 psi) necessary for detecting changes in biological ICP associated with brain swelling after TBI. The 3rd generation sensors were also to be smaller than previous versions and have small connector cables.

Several sensor development activities were employed to yield the first wafer-scale, absolute pressure sensor in a similar ultra-thin form factor as the original contact stress sensor. These sensors are still under development to meet the specific needs of the TBI study. Their thinness and unobtrusive packaging were to allow for ready insertion to numerous intracranial sites. To produce these sensors at a wafer scale, a new MEMS fabrication approach was developed and tested for the first time. For absolute pressure sensing, the contact stress sensor must be modified to create an improved reference volume cavity; a trapped volume of gas that is hermetically sealed within the device. The new process pre-defines the pressure sensor's reference cavity within the Silicon-on-Insulator (SOI) wafer. The pre-definition provides a variety of advantages to the overall process:

- The cavity definition requires a plasma etch that is a challenging operation to perform on a thinned substrate, performing this etch at the start of the SOI build

pushes the process to a thick-wafer operation simplifying the processing significantly

- Producing the reference cavity requires a hermetic seal that requires a high temperature operation that is difficult to perform later in the process once metals are on the substrate
- Pushing the cavity formation to the start of the process reduces yield risk by placing the most difficult process at the start of the fabrication (least substrate added-value)
- Pre-definition of the cavity paves the way for no backside processing of thinned substrate increasing the overall yield of the substrates
- Etching of the cavities prior to metallization keeps the etching process CMOS clean
- Commercialization of the sensor is aided by this process as use of CMOS-clean commercial foundries will not be restricted

In parallel with the wafer-scale absolute sensor process, several other important changes were initiated in parallel. The new process includes a CMOS-clean metal stack throughout the cleanroom processing. Similar to the non-metal etching mentioned above, maintenance of CMOS-clean metals allows any foundry to build the substrates. A major difficulty in finding commercial foundries to perform the sensor process was locating MEMS-specific foundries willing to work with our non-CMOS metals used to date. LLNL's clean room is not restricted by these metals but most external foundries are. A goal of this project was to identify and execute the process at an external foundry. This was pursued for two reasons, 1) there is a significant cost and time savings by performing this work externally and 2) use of an external foundry allows ready transfer of the technology to the commercial sector as LLNL cannot act as a commercial foundry. The CMOS-clean metals require modification of the solder joint with the package. LLNL attempted the modification by use of a solder-ball bumping process at a commercial vendor. Solder bumping is an industry standard and an established process. Adaptation of this process has some risk but if successful, will greatly reduce the packaging cost of the finished part. The cost savings is the result of application of the solder to the wafer scale (1000's of sensors at a time) vs. the package scale (10's of sensors at a time).

The solder bumping testing began with identification of the correct solder ball size to produce the needed solder bump height after reflow. Calculations identified the expected bump height based on the solder ball volume. The exact parameters were established by testing the designed solder ball volume on the defined bond-pad size (the bond-pad size dictates the solder reflow wetting area and thus the finished solder height). The designed pad size was bracketed above and below by 20 microns. The test run showed a robust outcome with all three pad sizes, each forming excellent solder joints with the test packages. Based on this study, a metal bond pad size was chosen and designed into the sensor photolithography masks.

Additional work was undertaken to investigate singulation of the silicon MEMS die by a cutting process in lieu of an etching process. With the pre-defined recesses in the SOI wafer, a backside process for the recess definition after wafer thinning was not required.

The other backside process used up to this time is plasma etch to singulate the die. If a substitute for this process can be identified, no backside processing will be required of the wafers. This represents an enormous cost savings and improved yield. Again, it allows the process to move forward in CMOS clean facilities. The obvious choice for singulation is a wafer saw process. We attempted to use a cutting die now to confirm that the edge roughness does not pose a fracture risk to the thinned die. As these sensors are exceptionally thin (~65 microns), their strength was a concern. A rough sidewall may facilitate chip cracking and device failure. We sent diced samples and etched samples to a private company to perform failure testing on a custom bending apparatus we are designing together. Development of this process continued to identify issues with this singulation technique. Alternatives were considered including laser dicing, sidewall polishing or reverting back to plasma etching.

To determine whether this process would weaken or compromise the chips, a series of tests were done to compare breaking strengths of plasma-defined and saw-defined chips. A private vendor (Corwil Technology) prepared saw-diced samples. The vendor is the same vendor that the fully executed process will use. These saw-diced samples were compared with LLNL-fabricated plasma-etched samples. The plasma-etched chips were formed with the identical process that has been used successfully for several years. The two populations were compared by performing failure testing in a custom bending apparatus. The results of the testing were exceptional: the cheaper and easier process (saw dicing) produced stronger chips. This outcome was very favorable. Details are shown in the following figures.

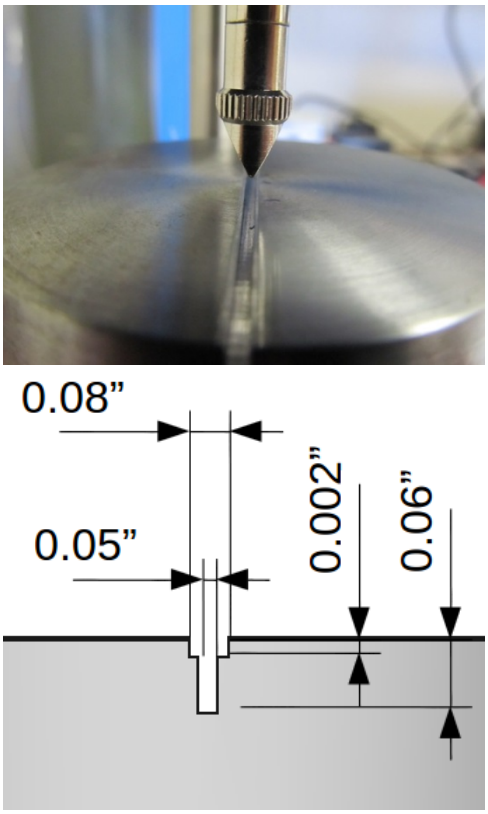

Figure 31. Chip cracking test configuration: Chips were tested under 3-point bending loading where a chip was put above linear cavity on a steel holder and loaded from the top with V-shaped chisel-like tip. Parameters and photograph of the test setup used for the chip cracking are shown in the upper figure and schematic dimensions in the lower figure.

Before the test a silicon chip was positioned above the cavity using vacuum tweezers (SMD-VAC-GP, Virtual Industries) with plastic tip. Then the chip was covered with silicone open-cell foam (0.062” thick, HT-870, Stockwell Elastomerics). The chip was loaded by slowly lowering the testing tip centered above the chip. Peak force was recorded and used as a breaking force.

Figure 32. Influence of thickness on break force: Results of break force measurements for saw-diced chips with different thicknesses are shown in the figure. SperScientific force gauge was used for these tests. It is clear from the figure that thicker samples have higher break force. This result indicates that testing technique used for the experiments is good enough for the purpose – it allows differentiating between samples with different properties.

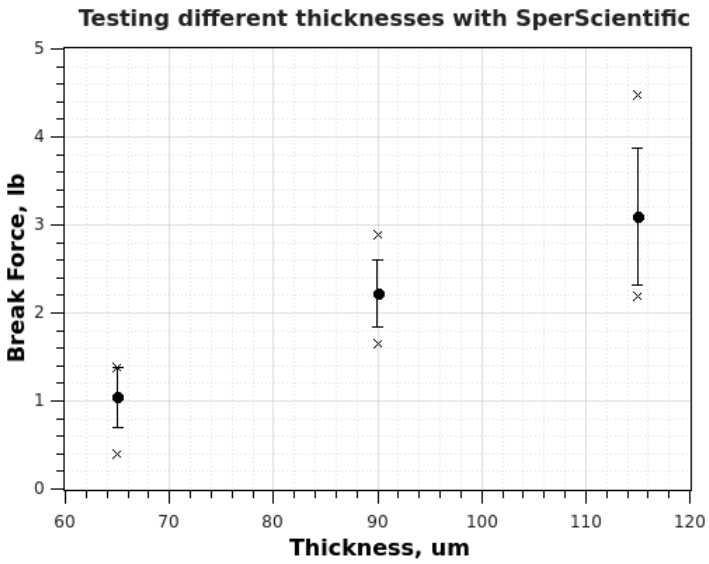

Figure 33. Plasma-etched chips vs. saw-diced chips: The graph compares the influence of plasma-etching and saw-dicing on chips mechanical strength. It is clear that saw-dicing is advantageous compared to plasma-etching.

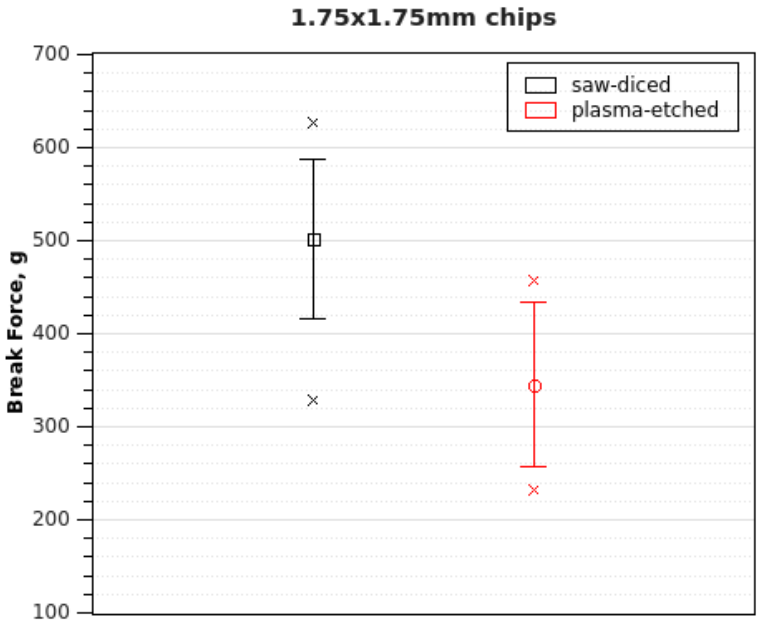

Conclusions from the chip cracking testing:

1. Saw-dicing is advantageous compared to plasma-etching for production of silicon chips with superior breaking strength.
2. Chip thickness has considerable effect on breaking strength – average breaking force measured in the experiments increases from about 1lb for 65 um chips to about 3 lb for 115 um chips (saw-diced).
3. Orientation of the chip (face-up or face-down) does not have significant effect on the breaking force that suggests about good quality of polishing procedure that does not affect mechanical strength of the chip.

Impact:

The current impact is minimal since we have not been able to produce a product that meets the goals of the project.

Changes/Problems:

The major objective of this research effort was to develop miniaturized, state-of-the-art pressure/temperature sensors to measure the immediate increases in ICP combined with longer-term measurements of biological ICP and intracranial temperature in animal models of TBI. The goal was to create new sensing technologies by modifying existing micro-electromechanical systems (MEMS) contract-stress pressure sensors developed at Lawrence Livermore National Laboratories (LLNL). Significant findings include the following. (1) We determined that the first generation original LLNL sensors required a sealed reference volume over the sensor diaphragm in order to reliably detect pressures in a wet environment across a range of impact and blast TBI pressures. (2) We modified the original sensors by epoxying an extremely thin layer of glass over the sensor diaphragm, creating a closed and sealed reference volume. This met with success in measuring fluid percussion impact pressures and accurate temperatures, but had an unacceptable increased size and also lacked sensitivity for measuring the relatively small biological ICP. (3) LLNL produced a second generation sensor with a closed reference volume, but was still not capable of measuring the lower pressures associated with biological ICP. Engineering calculations and static pressure testing determined that a thinner diaphragm should solve this problem by increasing sensitivity to lower pressures and reduce the overall dimensions of the sensor. (4) LLNL fabricated second generation sensors with a range of diaphragm diameters (200, 400, 600, 800, & 1000 μm). As the diameter of the diaphragm increases, sensitivity to lower pressures increases. These wafer-scale, absolute pressure sensors have an smaller form factor (thickness 90 μm prior to packaging and 130 μm after final packaging. (5) Fabrication of the re-engineered third generation sensors with the new wafer design and has been fraught with technical problems causing unfortunate delays.

Dr. Kotovsky at LLNL has been diligently working on re-engineering the design of the 3rd generation sensor to address the shortcomings described above. Dr. Kotovsky has met June, 2013 with the director of US sales for the company that we had planned to purchase wafers from for the new sensor chip build. Dr. Kotovsky worked on organizing the geometries to be included in that build. Those wafers were to be processed at Sandia National Laboratories in the wafer thinning house for the process development and chip build. The wafer purchase would include additional wafers needed for the development work. A quote for this work was received and we placed the order once our design geometry was complete. This required coordination with Sandia as their silicon patterning stepper drove some of the geometry choices for the build.

We discussed with a sub-contractor in Livermore who might be able to perform the packaging assembly work. Dr. Kotovsky worked with the sub-contractor on practice assemblies anticipating the new upcoming build. Working through an outside contractor represents an enormous cost savings for this fabrication work versus performing that work at LLNL. In the future, that company may also serve as a supplier for sensors to Walter Reed and other organizations.

We also discussed the process development risks with the wafer lapping company. The proposed change in the process to create buried diaphragms for TBI pressure sensing places the wafer at risk of mechanical failure. Dr. Kotovsky discussed these risks with the lapping vendor and believed we have a good chance of success but this remains our greatest risk.

After the first lot of pre-etched SOI wafers was built, they entered their remaining processing to define the ion implants and metal contacts to create the strain-sensitive circuit of the device. The vendor Icemos Inc. was selected for the continued processing. A long series of delays was discouraging. We subsequently worked to assist the vendor with their issues. In parallel, we continue to explore alternate vendors for future process runs as the delays have been unreasonable.

During the fall of 2014, a private company, Micrometrics Inc. (http://www.micrometricsinc.com/) licensed the intellectual property for the contact stress sensor. LLNL has been working closely with Micrometrics to assist the commercialization of the sensor. The lab was delighted to have a commercial path forward for ongoing access to the sensor by the DOD, DOE and parties interested in studying TBI.

Dr. Kotovsky continues to work on these issues with the foundry and future builds will use a new partner (Rogue Systems in Oregon) for the processes that have proved difficult with Icemos. Icemos will continue to support the wafer build, but the electronic elements will pass to Rogue Systems.

Dr. Kotovsky is planning to have more chips packaged from 20 micron thick diaphragm that may solve the low pressure detection problems. Micrometrics performed more low-pressure calibration work and shows promising returns from these devices although not as sensitive as 15um diaphragms. LLNL is also working on packaging challenges which are less of a concern than the chip issues which caused our greatest concerns and cost threat.

In summary, we have encountered numerous engineering and fabrication problems that stalled the progress of this project.

Products:

Second generation sensors were produced which could measure high pressure impact events, but failed to meet the requirements of also measuring pressure events (biological ICP). The dimensions of the second generation sensor are not optimal for in vivo measurements.

Dr. Kotovsky at LLNL is continuing to address the problems described elsewhere in this report and will make the third generation sensors available to the DoD if and when he is successful. LLNL continues to support the sensor work which ultimately will benefit the DoD.

Participants & Other Collaborating Organizations:

UC Davis participants:

Name:	Bruce Lyeth, PhD
Project Role:	Principle Investigator
Researcher Identifier:	252972781 (UC Davis ID)
Contribution to the project:	Dr. Lyeth supervised the project and wrote all reports

Name:	Gene Gurkoff
Project Role:	Postdoctoral fellow
Contribution to the project:	Dr. Gurkoff performed calibration of the sensors

Name:	Ken Van, MS
Project Role:	Technician
Contribution to the project:	Mr. Van performed the surgeries and histology

Name:	David Bonner
Project Role:	Graduate Student
Contribution to the project:	Mr. Bonner performed the glass cover slipping of the original sensors

LLNL participants (collaborating organization):

Lawrence Livermore National Laboratories
Livermore, CA

Name:	Jack Kotovsky, PhD
Project Role:	Sub award co-Investigator
Contribution to the project:	Dr. Kotovsky designed and fabricated the sensors

Name:	Erik Mukerjee, PhD
Project Role:	Sub award co-Investigator
Contribution to the project:	Dr. Mukerjee designed and fabricated the sensors

Name:	Angela Tooker, PhD
Project Role:	Postdoctoral fellow
Contribution to the project:	Dr. Tooker assisted Dr. Kotovsky in the fabrication of the sensors

Special Reporting Requirements:

None

Appendices:

None